Available online at www.sciencedirect.com
SCIENCE DIRECT
Catalysis Today 104 (2005) 360–371
CATALYSIS TODAY
www.elsevier.com/locate/cattod

Feasibility analysis of membrane reactors – discovery of reactive arheotropes

Yuan-Sheng Huang [a], Ernst-Ulrich Schlünder [a], Kai Sundmacher [a,b,*]

[a] *Max-Planck-Institute for Dynamics of Complex Technical Systems, Sandtorstrasse 1, D-39106 Magdeburg, Germany*
[b] *Otto-von-Guericke-University Magdeburg, Process Systems Engineering, Universitätsplatz 2, D-39106 Magdeburg, Germany*

Abstract

A feasibility analysis methodology adopted from reactive distillation is applied to membrane reactors. A model is formulated to depict the reactive liquid phase composition on the retentate side of a continuous type membrane reactor. The effects of both the chemical reaction kinetics and the membrane mass transfer kinetics on the feasible products are elucidated by means of retentate phase diagrams and bifurcation analysis. The proposed method can be applied to various membrane processes, independent of the specific structure of the membrane. Two quaternary reaction systems are considered to illustrate the methodology. In the first hypothetical system, it is shown how selective membranes can influence the sequence of effective volatilities which in turn affects the feasible products of the system. In the second example of practical importance, i.e. the heterogeneously catalysed synthesis of propyl acetate coupled with permeation through a porous polycarbonate membrane, the dusty gas model is applied to describe the component fluxes through the membrane. For the latter reaction system, the existence of *reactive arheotrope* is demonstrated. Arheotropes represent mass transfer controlled feasible products of membrane separation process.

Keywords: Membrane separation; Residue curve map; Bifurcation analysis; Feasibility; Dusty gas model; Esterification

1. Introduction

Membrane reactor, a hybrid process combining chemical reaction and membrane separation, can have several advantages such as to enhance conversion and reaction kinetics, to reduce operating costs and energy consumption, or to achieve in situ purification of the reaction mixture. In particular, membrane reactors can be a very promising alternative for systems which are incompatible with reactive distillation. Nevertheless, there are still a lot of challenges for membrane reactors despite their potential advantages. The first crucial hurdle is the property of the membranes. Generally speaking, the selectivity and permeability of real membrane materials are limited and usually contradictory to each other. Additionally, the stability and membrane fouling issues also make the membrane reactors less reliable than conventional reactors. To overcome these problems, in principle, requires synthesizing new membrane materials.

The second problem that retards the development of membrane reactors is concerned with engineering aspects. The complexity of process behavior in membrane reactors increases drastically due to the combination of chemical reaction and membrane transport. Thus, the majority of works on membrane reactors heretofore mainly performed experimental measurements, see e.g. [1–8]; some attempts have also been made to model membrane reactors [9–12]. But to the best of our knowledge, so far there is no systematic approach for the feasibility analysis of membrane reactors, i.e. to assess the influence of membrane mass transfer and the operating parameters on the attainable products for a given target reaction. In the literature, methodologies for the analysis, synthesis and control of membrane reactors have been rarely addressed.

In this work, in order to evaluate the attainable products of continuously operated membrane reactors, an approach adopted from distillation processes is generalized to be

Abbreviations: DGM, dusty gas model; MR, membrane reactor; PSPC, potential singular point curve; RCM, residue curve map; RD, reactive distillation

* Corresponding author. Tel.: +49 391 611 0351; fax: +49 391 611 0353.
E-mail address: sundmacher@mpi-magdeburg.mpg.de (K. Sundmacher).

0920-5861/$ – see front matter © 2005 Elsevier B.V. All rights reserved.
doi:10.1016/j.cattod.2005.03.076

Nomenclature

a	interfacial area per unit column length (m^2/m)
a_i	liquid phase activity of component i
A, B, C, D	chemical species
A_c	sectional area (m^2)
B_0	permeability constant of porous membranes, Eq. (18) (m^2)
$[B^e]$	the inverse matrix of $[k]$ in dusty gas model, Eq. (22a)
B^e_{ii}, B^e_{ij}	elements of $[B^e]$, Eqs. (22b) and (22c) $(m^2/s)^{-1}$
Da	Damköhler number, Eq. (8)
D_{ij}	binary diffusivity (m^2/s)
D^e_{ij}	effective binary diffusivity in porous media, Eq. (20) (m^2/s)
$D^e_{K,i}$	effective Knudsen diffusivity of i, Eq. (19) (m^2/s)
$[k]$	matrix of binary effective mass transfer coefficients, Eq. (14)
k_A	dimerization equilibrium constant, Eq. (32c)
k_f	forward reaction rate constant (s^{-1})
$k_{f,ref}$	forward reaction rate constant at reference temperature (s^{-1})
k_{ij}	effective binary mass transfer coefficients of pair i–j (m/s)
K	chemical equilibrium constant
L	total molar flow rate, Eq. (2) (mol/s)
L_i	component molar flow rate, Eq. (1) (mol/s)
M_i	molecular weight of component i
n_i	molar flux of component i through membrane (mol/m^2 s)
n_T	total molar flux through membrane (mol/m^2 s)
$n_{T,ref}$	total molar flux at a reference state (mol/m^2 s)
N_{ij}	interaction parameter for NRTL model, Eq. (31a)
NC	number of reacting species
p_i^{sat}	saturated vapor pressure of component i (bar)
P	system pressure (bar)
r	reaction rate (mol/(mol s))
R	universal gas constant (8.314 J/(mol K))
$\Re$	dimensionless reaction rate, Eq. (3)
t	time (s)
T	temperature (K)
x_i	liquid phase mole fraction of component i
X_i	transformed liquid phase mole fraction of component i, Eq. (10)
y_i	mole fraction of component i in vapor phase
Y_i	transformed vapor phase mole fraction of component i, Eq. (10)
z	axial coordinate of reactor column (m)
z_A, z_N	dimerization correction factor, Eqs. (32a) and (32b)
z^*	dimensionless axial coordinate, Eq. (7)

Greek letters

α_{ij}	relative volatility of i with respect to j, Eq. (25)
γ_i	liquid phase activity coefficient of component i
δ	membrane thickness (m)
ε	membrane porosity
ε_{cat}	catalyst loading density (mol catalyst)/m^3
θ	dimensionless axial variable, Eq. (11)
κ_{ij}	dimensionless binary mass transfer coefficient, Eq. (15b)
μ	viscosity of vapor mixture, Eq. (17)
ν_i	stoichiometric coefficient of component i
ν_T	total mole change of reaction
σ_{ij}	interaction parameter for NRTL model, Eq. (31b)
τ	tortuosity of membrane pores

Subscripts

A, B, C, D	components A, B, C and D, respectively
AcAc	acetic acid
H_2O	water
i, j	components i, j
p	permeation side
PrAc	propyl acetate
PrOH	propanol

applicable to membrane reactors. A model is formulated to describe the concentration profiles in the retentate liquid phase, in which the chemical reaction takes place, when vacuum is applied on the permeation side. Residue curve maps, or being more precise, ''retentate phase diagrams'' for membrane process, and bifurcation analysis are applied to elucidate the interaction of chemical reaction and membrane separation.

As extension of a previous study [13], in this work a continuously operated membrane reactor is considered. Two quaternary systems are studied as examples to illustrate the here proposed methodology. The first one is an ideal reactive mixture with constant relative volatilities, and the other is the esterification reaction of acetic acid with propanol. In the latter example, the dusty gas model is applied to describe the permeation of components through porous polycarbonate membranes. The general objective of this work is to develop a methodology such that the feasibility analysis of membrane reactors can be carried out directly based on the structural characterization of considered membranes.

2. Theory

2.1. Derivation of model equations

A continuous membrane reactor is considered as depicted in Fig. 1. The reaction is assumed to take place in the liquid

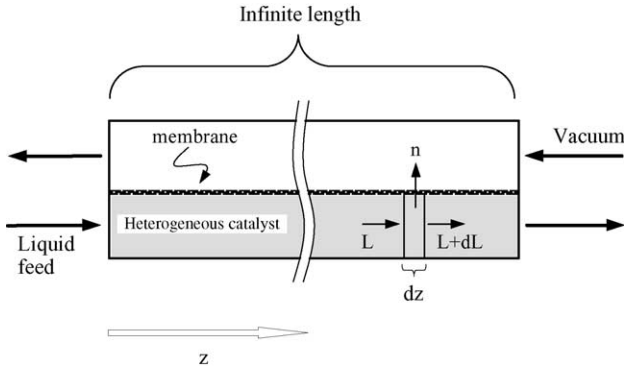

Fig. 1. Continuously operated membrane reactor.

retentate phase only. The membrane is assumed to be gas-filled with the vapor–liquid interface being placed at the retentate side of the membrane surface. At steady state, the component and overall material balance equations for any segment dz can be written as

$$L_i = L_i + \mathrm{d}L_i + n_i a\,\mathrm{d}z - A_c\,\mathrm{d}z\varepsilon_{cat}\nu_i r, \quad i = 1\cdots \mathrm{NC}-1 \tag{1}$$

$$L = L + \mathrm{d}L + n_T a\,\mathrm{d}z - A_c\,\mathrm{d}z\varepsilon_{cat}\nu_T r \tag{2}$$

where L_i stands for the component molar flow rate, L the total molar flow rate, n_i the molar flux through the membrane, $n_T = \sum_{i=1}^{NC} n_i$ the total molar flux, a the interfacial area per unit column length, A_c the cross sectional area, and ε_{cat} the catalyst loading density. ν_i is the stoichiometric coefficient, $\nu_T = \sum_{i=1}^{NC}\nu_i$ the total mole change of the chemical reaction. The chemical reaction rate, r, can be generally expressed as

$$r = k_f(T)\cdot \Re(x) \tag{3}$$

where k_f is the temperature-dependent rate constant of forward reaction, and $\Re$ denotes the dimensionless reaction rate which depends on the liquid phase composition. Eqs. (1) and (2) can be rewritten as

$$\frac{\mathrm{d}(Lx_i)}{\mathrm{d}z} = -n_i a + A_c\varepsilon_{cat}\nu_i k_f \Re, \quad i = 1\cdots \mathrm{NC}-1 \tag{4}$$

$$\frac{\mathrm{d}L}{\mathrm{d}z} = -n_T a + A_c\varepsilon_{cat}\nu_T k_f \Re \tag{5}$$

Rearranging the above equations and introducing the dimensionless Damköhler number Da yield:

$$\frac{\mathrm{d}x_i}{\mathrm{d}z^*} = \left(x_i - \frac{n_i}{n_T}\right) + Da(\nu_i - \nu_T x_i)\frac{n_{T,ref}}{n_T}\frac{k_f}{k_{f,ref}}\Re, \quad i = 1\cdots \mathrm{NC}-1 \tag{6}$$

where

$$\mathrm{d}z^* = \frac{n_T a}{L}\,\mathrm{d}z \tag{7}$$

stands for the dimensionless axial coordinate, $n_{T,ref}$ and $k_{f,ref}$ are the total molar flux and the forward reaction rate constant at a reference point within the composition space, respectively. The Damköhler number Da is defined as the ratio of the characteristic reaction rate and the characteristic permeation rate:

$$Da = \frac{A_c\varepsilon_{cat}k_{f,ref}}{n_{T,ref}a} \tag{8}$$

Eq. (6) describes the retentate concentration profile along the axial coordinate at steady state; it is equivalent to the dynamic mass balance of a corresponding batch process [13], except that the former process is expressed in terms of its axial coordinate, while the latter is expressed in terms of time. Depending on the Damköhler number, Eq. (6) describes non-reactive operation ($Da = 0$), chemical kinetics controlled operation ($0 < Da < \infty$), or chemical equilibrium controlled operation ($Da \to \infty$).

To transfer mass from the retentate phase through the membrane to the permeate side, heat has to be supplied to the process. As discussed in [14] for reactive distillation, different heating policies will influence the feasible products. In this work, an autonomous heating policy is applied in the first example of ideal system for the sake of concision, while an isothermal heating policy is applied to the second example of practical relevance. In the latter case, the temperature dependency of the forward rate constant is not relevant in Eq. (6). (In this case the lowest boiling component propanol is chosen as reference point for $n_{T,ref}$.)

2.2. Singular points and bifurcation analysis

The singular points of Eq. (6) are of special interest because those points structure the topology of the retentate phase diagrams. Thus, bifurcation analysis of these points yields fast information on the feasibility of a certain process variant. By introducing a new set of composition variables, Eq. (6) can be cast into an analogous form as in distillation:

$$\frac{\mathrm{d}X_i}{\mathrm{d}\theta} = X_i - Y_i, \quad i = 1\cdots \mathrm{NC}-1, \ \ i \neq k \tag{9}$$

where k marks a reference component. X_i, Y_i are the transformed liquid and vapor composition variables, being defined as following:

$$X_i = \frac{\nu_k x_i - \nu_i x_k}{\nu_k - \nu_T x_k}, \quad Y_i = \frac{\nu_k n_i - \nu_i n_k}{\nu_k n_T - \nu_T n_k}, \quad i = 1\cdots \mathrm{NC}-1, \ \ i \neq k \tag{10}$$

and θ as the new axial coordinate defined as

$$\mathrm{d}\theta = \frac{a(\nu_k n_T - \nu_T n_k)}{L(\nu_k - \nu_T x_k)}\,\mathrm{d}z \tag{11}$$

At the singular points the transformed vapor and liquid phase mole fraction are equal:

$$X_i = Y_i, \quad i = 1\cdots \mathrm{NC}-1, \ \ i \neq k \tag{12}$$

The compositions fulfilling Eq. (12) are called *reactive arheotropes* [13]. The arheotropic loci form a curve on which all singular points are located. Therefore, as in reactive distillation [15], this curve is called ''potential singular point curve'' (PSPC). The shape and location of the PSPC are determined by the reaction stoichiometry, the vapor–liquid phase equilibrium of the considered mixture, and the mass transfer properties of applied membrane.

2.3. Description of permeation through membranes

The validity of Eq. (6) is independent of the flux equation to be applied for a specific membrane which is under consideration. However, for feasibility analysis, adequate flux equations have to be formulated to close the set of governing equation. In the present work, two types of flux expressions are applied. First, for the considered ideal quaternary system, the permeation fluxes are expressed in terms of the partial pressure difference across the membrane. In the second example of practical importance, the permeation fluxes through the porous membrane are formulated by the dusty gas model.

2.3.1. Explicit expression of pressure-driven membrane permeation

Provided that the mass transfer resistance mainly exists within the membrane, the partial pressure at the retentate side of the membrane can be calculated by

$$p_i = y_i P = x_i \gamma_i p_i^{\mathrm{sat}} \tag{13}$$

In a partial pressure-driven membrane diffusion process, the NC-dimensional vector of molar fluxes through the membrane (n) can be expressed as

$$(n) = \frac{1}{RT}[k](yP - y_{\mathrm{p}}P_{\mathrm{p}}) \tag{14}$$

where $[k]$ is the NC × NC-dimensional matrix of effective binary mass transfer coefficients k_{ij}, y_{p} and P_{p} denote the vector of mole fractions and the total pressure on the membrane permeate side, respectively. It is convenient to formulate Eq. (14) in terms of dimensionless mass transfer coefficients κ_{ij} which are the ratios of the effective mass transfer coefficients k_{ij} related to a reference coefficient. Here, the first main diagonal element k_{11} is taken as reference coefficient. This yields:

$$(n) = \frac{1}{RT}k_{11}[\kappa](yP - y_{\mathrm{p}}P_{\mathrm{p}}) \tag{15a}$$

with

$$\kappa_{ij} \equiv \frac{k_{ij}}{k_{11}} \tag{15b}$$

When vacuum is applied on the permeate side, the partial pressures of the diffusing components on the permeate side are negligible ($P_{\mathrm{p}} \to 0$). Then, Eq. (15a) becomes

$$(n) = \frac{P}{RT}k_{11}[\kappa](y) \tag{16}$$

In Eq. (16), membrane properties are reflected by the $[\kappa]$-matrix. Different membrane material structures (e.g. pore size), lead to different $[\kappa]$-matrices as discussed in [13]. In practice, the elements of the $[\kappa]$-matrix can depend on the process variables (e.g. y_i or P); nevertheless, for the sake of a simplified analysis, in the first system being considered here, $[\kappa]$-matrices with constant elements are used to elucidate the effects of membrane.

2.3.2. Mass transfer through porous membranes

The dusty gas model (DGM) is a well-established tool to quantify the flux of components through porous membranes [16,17]. This model is based on the Maxwell–Stefan equations, in which the porous medium is considered as the (NC + 1)th component with infinite molar mass and zero flux. The flux equation for species i in a NC-component mixture can be derived as

$$-\frac{1}{RT}\nabla p_i - \frac{1}{RT}\frac{B_0 p_i}{\mu D^{\mathrm{e}}_{\mathrm{K},i}}\nabla P = \sum_{j=1}^{\mathrm{NC}}\frac{y_j n_i - y_i n_j}{D^{\mathrm{e}}_{ij}} + \frac{n_i}{D^{\mathrm{e}}_{\mathrm{K},i}} \tag{17}$$

with $\quad i = 1 \cdots \mathrm{NC}$

Eq. (17) accounts for three transport mechanisms, namely bulk diffusion, Knudsen diffusion and viscous flow. B_0 is the permeability constant of the porous membrane

$$B_0 = \frac{\varepsilon}{\tau}\frac{d_{\mathrm{p}}^2}{32} \tag{18}$$

and $D^{\mathrm{e}}_{\mathrm{K},i}$ stands for the effective Knudsen diffusivity

$$D^{\mathrm{e}}_{\mathrm{K},i} = \frac{\varepsilon}{\tau}\frac{d_{\mathrm{p}}}{3}\sqrt{\frac{8RT}{\pi M_i}} \tag{19}$$

where d_{p} is the pore diameter, M_i the molar mass, ε and τ are the porosity and the tortuosity of the membrane, respectively. D^{e}_{ij}, the effective binary diffusivity in the porous medium, is related to the corresponding free space value by

$$D^{\mathrm{e}}_{ij} = \frac{\varepsilon}{\tau}D_{ij} \tag{20}$$

where D_{ij} is calculated by Fuller's method [18]. μ is the viscosity of the mixture, which is calculated by the methods of Reichenberg (viscosity of pure substances) and Wilke [18].

The membrane is assumed to be fully filled with vapor, i.e. the pressure on the retentate side of the membrane is calculated as the saturated vapor pressure of the liquid mixture, while the permeate side pressure is negligible if vacuum is applied. The pressure within the membrane is taken as the average value of the pressures on both sides.Eq. (17) can be cast into an explicit NC-dimensional matrix form as:

$$(n_i) = -\frac{1}{RT}[k]\left(\Delta p_i + \frac{y_i P B_0}{\mu D^{e}_{K,i}}\Delta P\right) \tag{21}$$

where

$$[k] = \frac{[B^{e}]^{-1}}{\delta} \tag{22a}$$

with δ as membrane thickness. The elements of the $[B^{e}]$-matrix are given by

$$B^{e}_{ii} = \frac{1}{D^{e}_{K,i}} + \sum_{j=1, j\neq i}^{NC} \frac{y_j}{D^{e}_{ij}} \tag{22b}$$

$$B^{e}_{ij} = -\frac{y_i}{D^{e}_{ij}} \tag{22c}$$

Based on Eqs. (21) and (22a)–(22c) it can be seen that the dusty gas model is equivalent to a non-diagonal $[\kappa]$-matrix (in Eq. (16)) whose elements are functions of the state variables, i.e. the vapor phase composition, y_i.

3. Results and discussion

3.1. Example I: ideal quaternary system

As first example, the effect of a selective membrane on the quaternary mixture A/B/C/D undergoing a single reversible chemical reaction in the ideal liquid phase is considered:

$$\mathrm{A} + \mathrm{B} \Leftrightarrow \mathrm{C} + \mathrm{D}, \quad \mathrm{C}: \text{ main product}, \quad \mathrm{D}: \text{ byproduct} \tag{23}$$

The dimensionless rate of the chemical reaction obeys the kinetic law

$$\Re = x_A x_B - \frac{x_C x_D}{K} \tag{24}$$

with K as chemical equilibrium constant.

For the sake of a simplified analysis, the following assumptions are made:

- The chemical equilibrium constant is independent of temperature: $K = 12$.
- The rate constant k_f is independent of temperature: $k_f/k_{f,ref} = 1$.
- The relative volatilities are assumed to be constant, and denoted as α_{BA}, α_{CA}, α_{DA} with respect to the reactant A. Therefore, the vapor phase equilibrium composition can be calculated as

$$y_i = \frac{\alpha_{iA} x_i}{\sum_{m=A}^{D} \alpha_{mA} x_m} \tag{25}$$

3.1.1. Retentate phase diagram

The effect of a membrane being integrated into a chemical reactor can be elucidated with the help of retentate phase diagrams, i.e. phase portraits of the liquid phase composition. As previously mentioned [13], distillation can be interpreted as a limiting case of a membrane process with the mass transfer matrix $[\kappa]$ being the identity matrix, i.e. no selective mass transfer effects. The applied volatility values are $\alpha_{BA} = 1.7$, $\alpha_{CA} = 3.9$, and $\alpha_{DA} = 4.2$, so that the reactants A and B are higher boilers than the products C and D. The quaternary mixture with this set of volatilities was also studied by [19,20] for non-reactive distillation and equilibrium controlled reactive distillation. Here, we consider this system for the purpose of comparison with a membrane reactor to see the effects of incorporating membranes.

Fig. 2 shows residue curve maps for the classical reactive distillation process at three different Damköhler numbers. In the non-reactive case ($Da = 0$, Fig. 2a), the map topology is structured by one unstable node (pure D), two saddle points (pure B and pure C) and one stable node (pure A). The arrows along the residue curves indicate the composition change along the axial direction. Since pure A is the only stable node of non-reactive distillation, this is the feasible bottom product to be expected in a continuous distillation column.

At kinetically controlled chemical reaction ($Da = 1$, Fig. 2b), there appears another saddle point (kinetic azeotrope), while pure C becomes an unstable node and B becomes a stable node. The quaternary saddle point forms two boundaries with the unstable nodes C and D such that the residue curves originate from C and D move towards the saddle point and eventually converge to A and B, respectively.

When the reaction rate is much faster than the permeation rate ($Da \rightarrow \infty$, Fig. 2c), the reaction approaches its chemical equilibrium, and therefore the quaternary saddle point (called *reactive azeotrope*) reaches the equilibrium surface (as shown later in Fig. 5 or 6). In this case, the residue curves are first dominated by the reaction stoichiometry and then move along the equilibrium surface converging to the stable nodes A and B.

By the proposed method, the retentate phase diagrams of the membrane reactors can be determined from Eq. (6) analogously. First, a diagonal $[\kappa]$-matrix is considered with $\kappa_{CC} = 0.8$, i.e. the membrane is slightly selective so that it retains the product C more than the other three components which are assumed to have the same mass transfer coefficients. Fig. 3a shows the phase diagram of such a membrane process at non-reactive condition ($Da = 0$). Due to the low selectivity of membrane, it does not change the sequence of relative volatilities. Thus, the topology of Fig. 3a is similar to Fig. 2a.

At kinetically controlled conditions ($Da = 1$, Fig. 3b), it again shows an additional quaternary saddle point (called *kinetic arheotrope*), and pure B becomes the stable node.

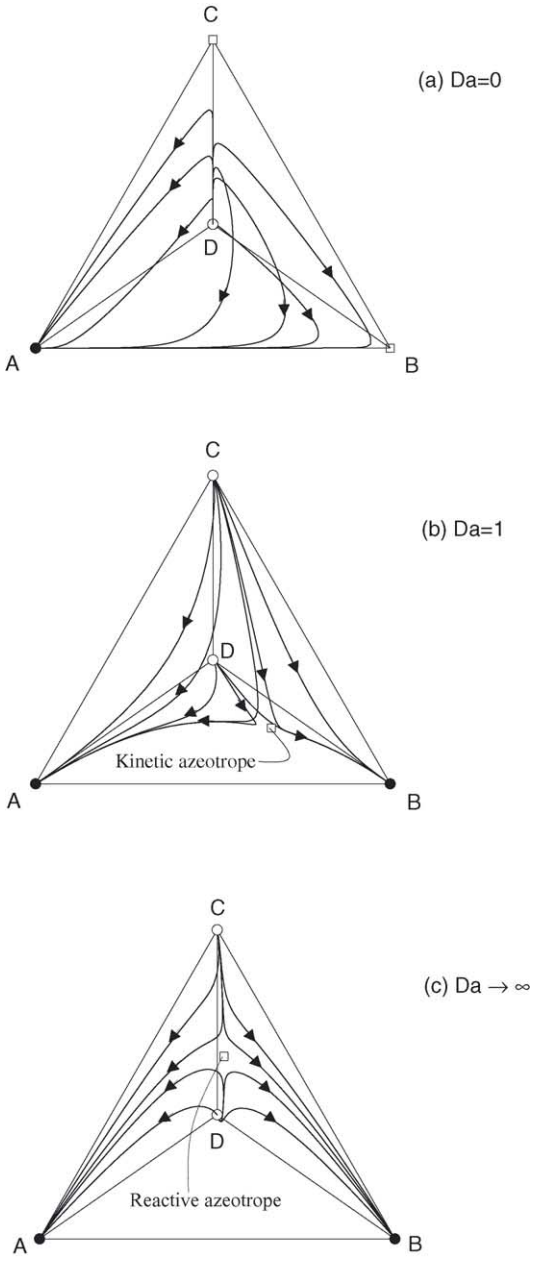

Fig. 2. Residue curve maps for reactive distillation; A + B ⇔ C + D; $K = 12$; constant relative volatilities: $\alpha_{BA} = 1.7$; $\alpha_{CA} = 3.9$; $\alpha_{DA} = 4.2$: (○) unstable node, (□) saddle point, (●) stable node; (a) no chemical reaction (i.e. non-reactive distillation), (b) kinetically controlled chemical reaction, (c) equilibrium controlled chemical reaction.

Different from Fig. 2b, the C vertex remains the saddle point. The unstable D forms two boundaries with the two saddle points, pure C and the just mentioned kinetic arheotrope. The composition trajectory lines originate from the D vertex, move towards the C vertex and the quaternary saddle point, and finally end up at pure A or pure B.

At infinite Damköhler number ($Da \rightarrow \infty$, Fig. 3c), the saddle point (called *reactive arheotrope*) is located exactly on the chemical equilibrium surface. The C vertex becomes the unstable node when the Damköhler number exceeds a critical value. The composition trajectory lines again move along the equilibrium surface and converge to the stable nodes A or B, similar to Fig. 2c, while the location of the reactive arheotrope is closer to the C vertex than the reactive azeotrope in Fig. 2c.

When the membrane is more selective, e.g. $\kappa_{CC} = 0.2$, the membrane changes the sequence of effective volatilities. Thus, C becomes the stable node, A and B are the saddle points and D remains the unstable node at any Damköhler numbers (as shown in Fig. 3d–f). The reaction kinetics in this case can only influence the composition trajectory, but not the location and stability of singular points. For the non-reactive case (Fig. 3d, $Da = 0$), the composition trajectory lines may spiral and travel through the whole composition tetrahedron; for $Da \rightarrow \infty$, the composition trajectory lines are constrained by the chemical equilibrium relationship so that they can only approach the equilibrium surface by the reaction stoichiometry first, and then move on the surface, i.e. the system loses a degree of freedom in the chemical equilibrium controlled case.

3.1.2. Singular point analysis

As revealed in the previous figures, the topology of retentate phase diagrams can be structured by the singular points. Thus, singular point analysis yields the key information on the feasibility of a membrane reactor. As mentioned in Section 2.2, all potential singular points of a certain system are located on a unique curve (PSPC) whose location is fixed by Eq. (12). For the considered quaternary case, the PSPC is determined by solving the following set of equations simultaneously:

$$X_A = Y_A \tag{26a}$$

$$X_B = Y_B \tag{26b}$$

where the main product C is chosen as the reference component. Eqs. (26a) and (26b) are the arheotropic conditions for the considered reaction example.

In Fig. 4, the PSPC for $\kappa_{CC} = 0.8$ (cf. Fig. 3a–c) is plotted as the intersection of the two surfaces described by Eqs. (26a) and (26b). Only the PSPC branch within the physically relevant composition space is shown here. A certain subset of points along the PSPC are singular points of physical relevance, i.e. for $Da \in [0,\infty]$. Points which correspond to negative Da-numbers are physically not relevant.

At the given set of relative volatilities, the PSPC of the distillation process is depicted in Fig. 5. For completeness, the PSPC is also shown outside the composition space. One branch of the PSPC passes through the composition tetrahedron and connects the B, C vertices. The quaternary saddle point emerges from the B vertex and moves along this PSPC branch with the increasing Damköhler number. It intersects the equilibrium surface and thus results in the reactive azeotrope at $Da \rightarrow \infty$. As for the pure component vertices, A and D remain the stable and unstable nodes, respectively, at any Damköhler number, while B changes

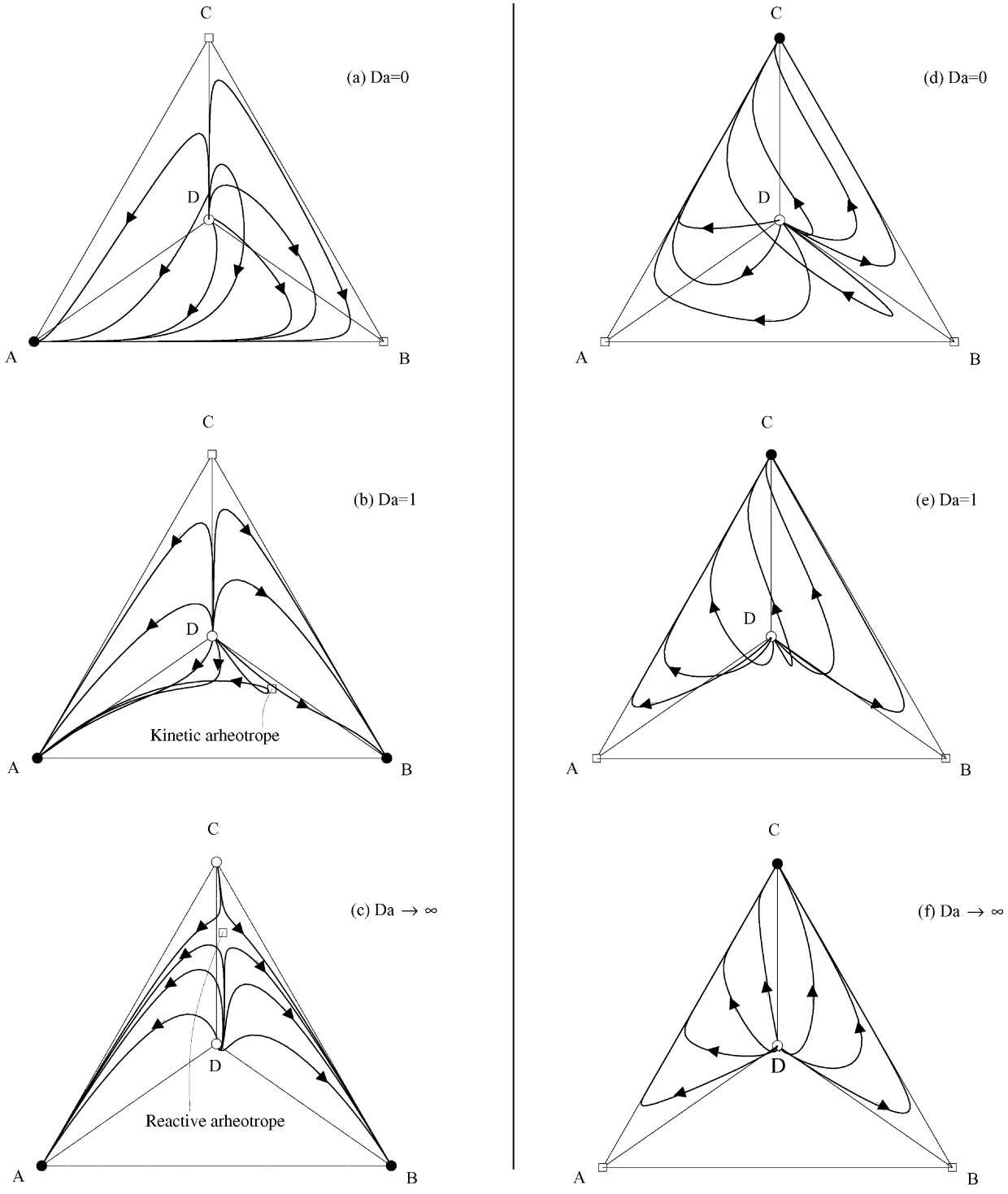

Fig. 3. Retentate phase diagrams for membrane reactor; A + B ⇔ C + D; $K = 12$; constant relative volatilities: $\alpha_{BA} = 1.7$; $\alpha_{CA} = 3.9$; $\alpha_{DA} = 4.2$: (○) unstable node, (□) saddle point, (●) stable node; (a–c) $[\kappa] = \begin{bmatrix} 1 & 0 & 0 & 0 \\ 0 & 1 & 0 & 0 \\ 0 & 0 & 0.8 & 0 \\ 0 & 0 & 0 & 1 \end{bmatrix}$, (d–f) $[\kappa] = \begin{bmatrix} 1 & 0 & 0 & 0 \\ 0 & 1 & 0 & 0 \\ 0 & 0 & 0.2 & 0 \\ 0 & 0 & 0 & 1 \end{bmatrix}$.

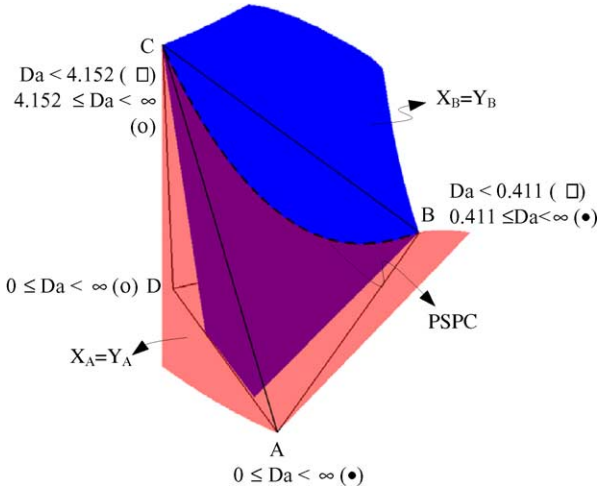

Fig. 4. Reactive arheotropic conditions and potential singular point curve (PSPC); A + B ⇔ C + D; $K = 12$; constant relative volatilities: $\alpha_{BA} = 1.7$; $\alpha_{CA} = 3.9$; $\alpha_{DA} = 4.2$; $\kappa_{CC} = 0.8$: (○) unstable node, (□) saddle point, (●) stable node, (- - -) PSPC.

from a saddle point to a stable node if $Da > 0.411$. The pure C vertex is a saddle point when $Da < 0.921$, and turns into an unstable node if the Damköhler number exceeds the critical value.

Similarly, the PSPCs of membrane reactors for the conditions given in Fig. 3a–c and d–f are depicted in Fig. 6a and b. For $\kappa_{CC} = 0.8$ (Fig. 6a), the shape of the PSPC is similar to Fig. 5, but the branch passing through the composition space is closer to the B–C edge. This leads to different locations for kinetic and reactive arheotropes compared to the azeotropes in the reactive distillation process. Furthermore, the pure C vertex is an unstable node in Fig. 2b, but a saddle point in Fig. 3b, because the critical

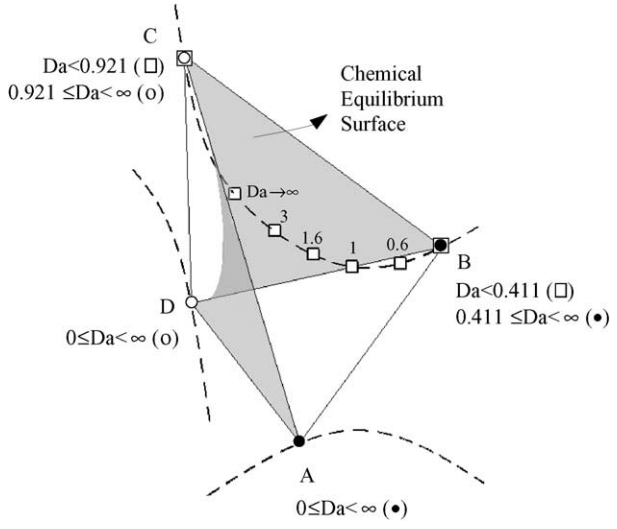

Fig. 5. Potential singular point curve (PSPC) and bifurcation behavior for reactive distillation; A + B ⇔ C + D; $K = 12$; constant relative volatilities: $\alpha_{BA} = 1.7$; $\alpha_{CA} = 3.9$; $\alpha_{DA} = 4.2$: (○) unstable node, (□) saddle point, (●) stable node, (- - -) PSPC.

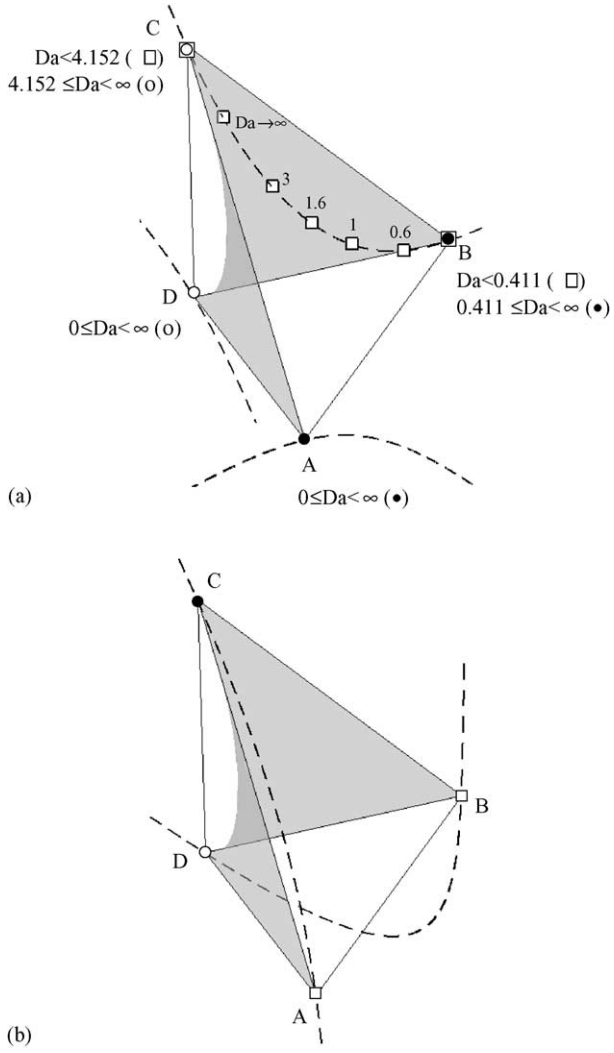

Fig. 6. Potential singular point curve (PSPC) and bifurcation behavior for membrane reactor; A + B ⇔ C + D; $K = 12$; constant relative volatilities: $\alpha_{BA} = 1.7$; $\alpha_{CA} = 3.9$; $\alpha_{DA} = 4.2$; (a) $\kappa_{CC} = 0.8$, (b) $\kappa_{CC} = 0.2$: (○) unstable node, (□) saddle point, (●) stable node, (- - -) PSPC.

value for pure C turning from a saddle point into an unstable node is $Da = 4.152$ in Fig. 6a. For $\kappa_{CC} = 0.2$ (Fig. 6b), both branches of the PSPC do not move into the composition tetrahedron, but only intersect the four pure component vertices. For this case, A and B are saddle points, C is the stable node and D is the unstable node permanently.

For the selection of suitable membrane materials, it is helpful to track the location of the feasible product composition in dependence on the membrane mass transfer coefficients. For instance, Fig. 7 shows the bifurcation behavior with respect to the relative mass transfer coefficient κ_{CC}. At equilibrium controlled conditions (i.e. $Da \rightarrow \infty$), the quaternary singular point moves from the reactive azeotrope ($\kappa_{CC} = 1$) towards the B–C edge as shown in Fig. 7a. When κ_{CC} is smaller than the critical value 0.436 ($=\alpha_{BA}/\alpha_{CA}$), the quaternary branch vanishes within the composition space, and pure B changes from a stable node into a saddle point, while pure C from an unstable into a

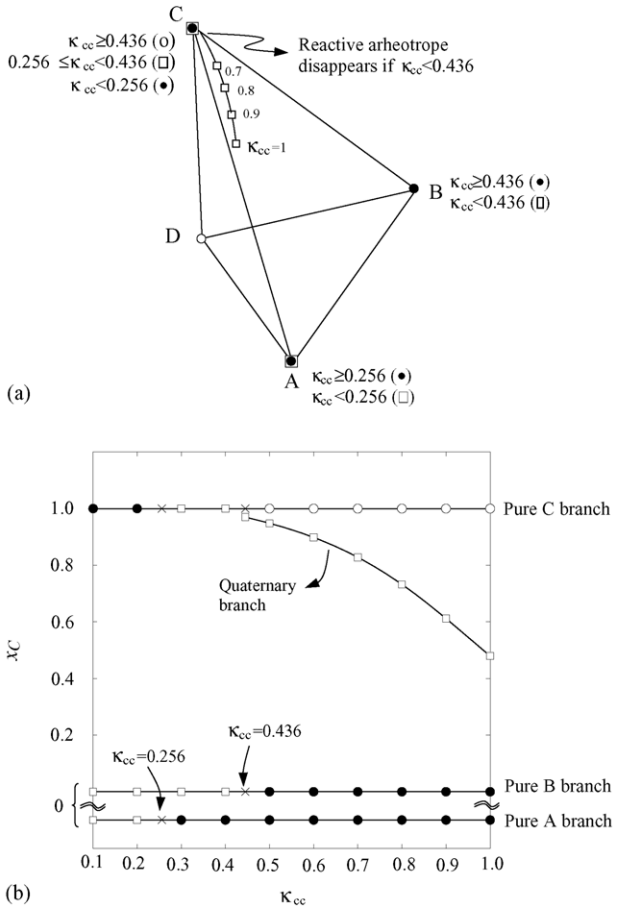

Fig. 7. Bifurcation behavior with respect to κ_{CC} (at $Da \to \infty$); A + B ⇔ C + D; $K = 12$; constant relative volatilities: $\alpha_{BA} = 1.7$; $\alpha_{CA} = 3.9$; $\alpha_{DA} = 4.2$: (○) unstable node, (□) saddle point, (●) stable node; (a) within the composition tetrahedron, (b) x_C versus κ_{CC}.

saddle point. When κ_{CC} becomes smaller than the value 0.256 (=$1/\alpha_{CA}$), C becomes the only stable node of the system, replacing the original stable node which was pure A (as in Fig. 7b).

3.2. Example II: non-ideal quaternary system

Now a non-ideal reaction system of technical relevance is considered: the synthesis reaction of propyl acetate, coupled with the permeation through porous polycarbonate membranes. This system was chosen mainly for two reasons: (i) to show how a realistic permeation model (dusty gas model) can be implemented in the frame of the proposed methodology, and (ii) to give a technically relevant example for the existence of a *reactive arheotrope*. As mentioned in Section 2.3.2, the [κ]-matrix of the dusty gas model is a non-diagonal matrix and its elements are functions of the composition.

The esterification reaction of acetic acid with propanol reads as:

$$\text{acetic acid (1)} + \text{propanol (2)} \xleftrightarrow{H^+} \text{propyl acetate (3)} + \text{water (4)} \tag{27}$$

A quasi-homogeneous rate approach is used for the reaction kinetics. The rate is expressed in terms of activities to account for the non-ideal mixing behavior of the reaction components in the liquid phase:

$$r = k_f \left(x_{AcAc}\gamma_{AcAc} x_{PrOH}\gamma_{PrOH} - \frac{x_{PrAC}\gamma_{PrAC} x_{H_2O}\gamma_{H_2O}}{K} \right) \tag{28}$$

To approach a realistic operation, the membrane reactor is considered at isothermal condition so that the temperature dependency of the rate constant k_f is not relevant. The equilibrium constant of the given reaction was experimentally determined within the temperature range 80–110 °C: $K = 20$ [14].

Taking into account the dimerization reaction of acetic acid in the vapor phase, the vapor mole fraction y_i can be calculated by [19,21]:

$$y_i P z_i = x_i \gamma_i(x_j, T)\, p_i^{sat}(T) \tag{29}$$

where the saturated pressures (Pa) are calculated as follows:

$$\ln(p_1^{sat}/[\text{Pa}]) = 22.1001 - \frac{3654.62}{T - 45.392} \tag{30a}$$

$$\ln(p_2^{sat}/[\text{Pa}]) = 22.72435 - \frac{3310.394}{T - 74.687} \tag{30b}$$

$$\ln(p_3^{sat}/[\text{Pa}]) = 21.6266 - \frac{3249.98}{T - 52.84} \tag{30c}$$

$$\ln(p_4^{sat}/[\text{Pa}]) = 23.2256 - \frac{3835.18}{T - 45.343} \tag{30d}$$

The liquid phase activity coefficients γ_i are estimated by means of the NRTL equation using the interaction parameters N_{ij} and σ_{ij} as listed below [22]:

$$\begin{bmatrix} N_{11} & N_{12} & N_{13} & N_{14} \\ N_{21} & N_{22} & N_{23} & N_{24} \\ N_{31} & N_{32} & N_{33} & N_{34} \\ N_{41} & N_{42} & N_{43} & N_{44} \end{bmatrix} = \begin{bmatrix} 0 & -147.4298 & -410.3887 & -342.1961 \\ 104.1007 & 0 & 1055.3593 & 152.5084 \\ 1050.5581 & -433.1348 & 0 & 720.1784 \\ 1175.7145 & 1866.3369 & 3497.7669 & 0 \end{bmatrix} \tag{31a}$$

$$\begin{bmatrix} \sigma_{11} & \sigma_{12} & \sigma_{13} & \sigma_{14} \\ \sigma_{21} & \sigma_{22} & \sigma_{23} & \sigma_{24} \\ \sigma_{31} & \sigma_{32} & \sigma_{33} & \sigma_{34} \\ \sigma_{41} & \sigma_{42} & \sigma_{43} & \sigma_{44} \end{bmatrix} = \begin{bmatrix} 0 & 0.3007 & 0.2970 & 0.2952 \\ 0.3007 & 0 & 0.3011 & 0.3747 \\ 0.2970 & 0.3011 & 0 & 0.2942 \\ 0.2952 & 0.3747 & 0.2942 & 0 \end{bmatrix} \tag{31b}$$

The dimerization correction factor z_i in Eq. (29) is calculated as following:

$$z_A = \frac{1 + (1 + 4k_A p_1^{sat})^{0.5}}{1 + (1 + 4k_A P y_A (2 - y_A))^{0.5}} \quad (32a)$$

for the associating molecule (acetic acid), and

$$z_N = \frac{2(1 - y_A + (1 + 4k_A P y_A (2 - y_A))^{0.5})}{(2 - y_A)(1 + (1 + 4k_A P y_A (2 - y_A))^{0.5})} \quad (32b)$$

for the other three components, where the dimerization equilibrium constant k_A (Pa^{-1}) is calculated from

$$\log_{10}(k_A) = -12.5459 + \frac{3166.0}{T} \quad (32c)$$

For separation, a polycarbonate membrane is considered here; this membrane is a commercially available product which is manufactured by track-etched processes. Thus, the membrane pores are nearly cylindrical ($\tau = 1$). The membrane thickness is reported to be 6 μm and the membrane porosity is 1.1% being calculated from the reported pore density. A pore diameter of 0.05 μm is assumed. The permeation of molecules through the here specified membrane is described by the dusty gas model. In practice, it will be important to avoid capillary condensation of the permeating vapor within the membrane pores. This can be achieved by an extra heat supply to the membrane.

3.2.1. Retentate phase diagram

To be concise, the RCM of distillation process will not be depicted in this work. For the purpose of comparison, the readers are referred to [14]. Fig. 8a shows the retentate phase diagram for the non-reactive membrane process at 105 °C. There are three non-reactive binary arheotropes in the retentate diagram. The arheotrope between propyl acetate and water (Ar 1) is an unstable node, while the other two (Ar 2, Ar 3) are saddle points. Pure propanol, propyl acetate and water are also saddle points, while acetic acid is the only stable node at given conditions. Composition trajectory lines originate from the unstable node, first approaching the saddle points, and eventually converging to the stable node. All singular points are also listed in Table 1.

If $Da = 1$ (Fig. 8b), Ar 2 and Ar 3 still keep their locations and stabilities, but the unstable node (Ar 1) no longer exists since propyl acetate and water start to react. Instead, the unstable node moves into the composition tetrahedron and becomes a quaternary unstable node (kinetic arheotrope). Moreover, the propanol apex turns to be a stable node instead of a saddle point.

At $Da \to \infty$ (Fig. 8c), chemical equilibrium is established and the composition trajectories first approach the equilibrium surface (as shown in [14]) following the reaction stoichiometry, and then move along this surface to the stable nodes A or B. The unstable node meets a saddle point branch, which emerges from the propanol/water edge (for $Da > 5.71$), on the equilibrium surface and results in the quaternary reactive arheotrope.

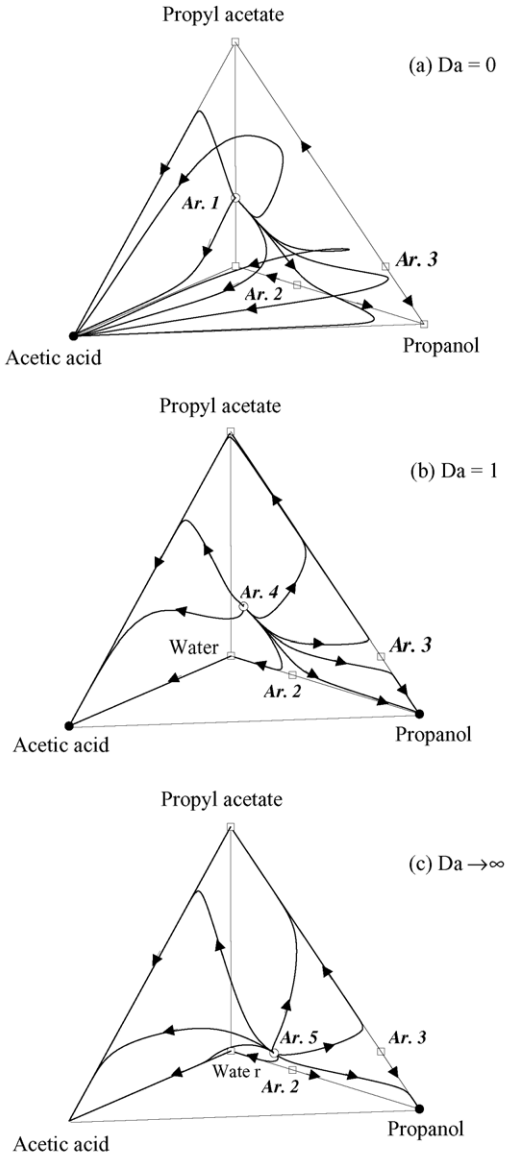

Fig. 8. Retentate phase diagrams for propyl acetate synthesis reaction coupled with permeation through polycarbonate membrane of 50 nm pore diameter at 105 °C. Ar = (reactive or kinetic) arheotrope: (○) unstable node, (□) saddle point, (●) stable node; (a) no chemical reaction, (b) kinetically controlled chemical reaction, (c) equilibrium controlled chemical reaction.

3.2.2. Singular point analysis

Fig. 9 shows the bifurcation behavior of the considered membrane reactor. The binary arheotrope between propyl acetate and water, Ar 1, moves into the composition tetrahedron when chemical reaction takes place ($Da > 0$). On the other hand, the binary arheotropes propanol/water (Ar 2) and propanol/propyl acetate (Ar 3), remain

Table 1
List of singular points in Figs. 8–10

Name	Composition	Type	Pressure (bar)	*Da*			x_1	x_2	x_3
				0	1	∞			
Arheotrope 1	$PrAc/H_2O$	Unstable	2.40	√			0	0	0.3125
Arheotrope 2	$PrOH/H_2O$	Saddle	1.92	√	√	√	0	0.3412	0
Arheotrope 3	PrOH/PrAc	Saddle	1.44	√	√	√	0	0.8012	0.1988
Arheotrope 4	$AcAc/PrOH/PrAc/H_2O$	Unstable	2.33		√		0.0174	0.0849	0.2499
Arheotrope 5	$AcAc/PrOH/PrAc/H_2O$	Unstable	2.06			√	0.0533	0.2854	0.0752
Propanol	PrOH	Saddle/stable	1.35	√	√	√	0	1	0
Water	H_2O	Saddle	1.20	√	√	√	0	0	0
Propyl acetate	PrAc	Saddle	1.13	√	√	√	0	0	1
Acetic acid	AcAc	Stable	0.67	√	√	√	1	0	0

unchanged at reactive conditions since these binary pairs do not react with each other. However, a saddle point branch emerges from Ar 2 when $Da > 5.71$, and then meets the unstable node branch at the reactive arheotrope ($Da \rightarrow \infty$). The other singular points remain their positions and stability at any *Da*, except that pure propanol changes from a saddle point to a stable node if *Da* exceeds the critical value 0.89.

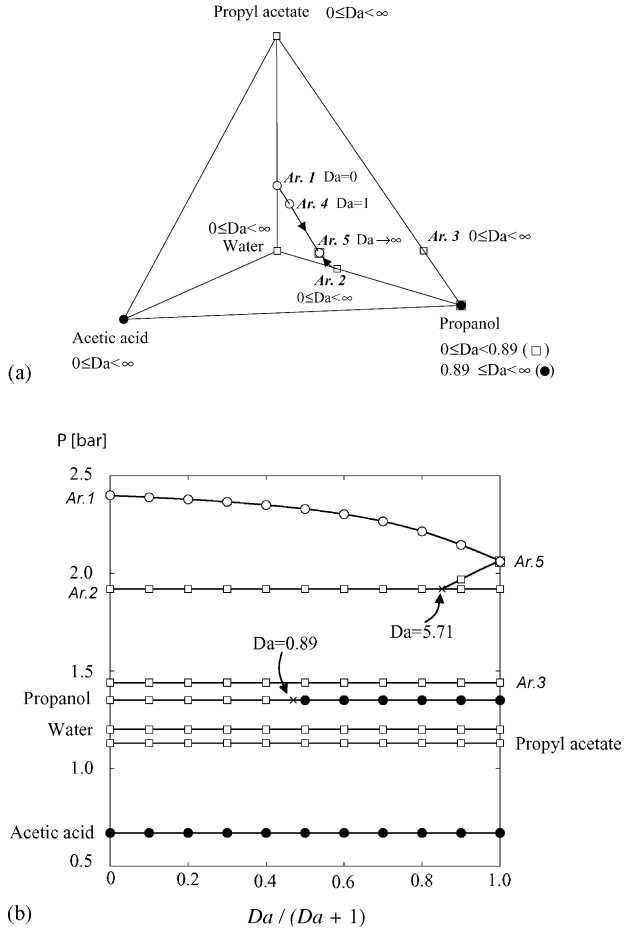

Fig. 9. Potential singular point curve and bifurcation behavior for propyl acetate synthesis reaction coupled with permeation through polycarbonate membrane of 50 nm pore size at 105 °C. Ar = (reactive or kinetic) arheotrope: (○) unstable node, (□) saddle point, (●) stable node; (a) within the composition tetrahedron, (b) pressure versus normalized Damköhler number.

Fig. 9b also shows the bifurcation behavior in terms of the system pressure versus the normalized Damköhler number, $Da/(Da + 1)$. It reveals that in the non-reactive case, Ar 1 is the lowest boiler and therefore is the unstable node, while acetic acid has the lowest pressure and is a stable node. With increasing Damköhler number, Ar 1 moves towards the reactive arheotrope (Ar 5). For $Da > 0.89$ propanol becomes another stable node in addition to acetic acid. For $Da > 5.71$, there appears another quaternary arheotrope as a saddle point, which joins the reactive arheotrope eventually at $Da \rightarrow \infty$.

For the considered porous membranes, the pore diameter d_p is the most important property which can be changed to influence the selectivity. Thus, a bifurcation analysis was performed with respect to the pore diameter (see Fig. 10). At chemical equilibrium controlled operation ($Da \rightarrow \infty$), there are two binary arheotrope branches between propanol/propyl acetate and propanol/water, and a quaternary branch.

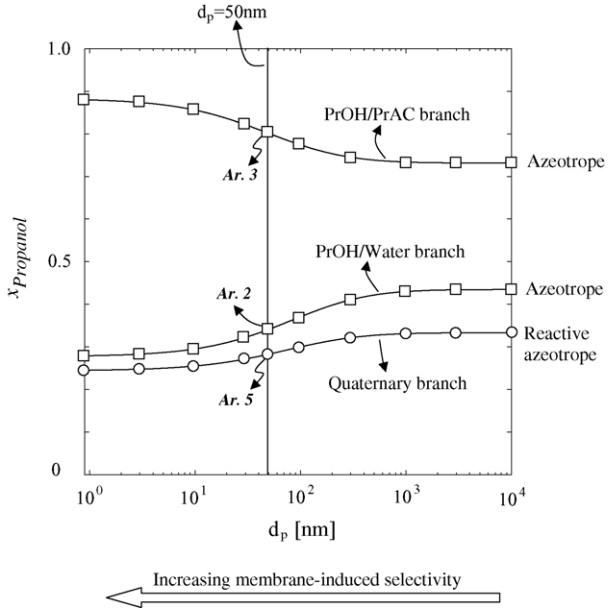

Fig. 10. Bifurcation behavior with respect to pore diameter (at $Da \rightarrow \infty$) for propyl acetate synthesis reaction coupled with permeation through polycarbonate membrane at 105 °C. Ar = (reactive or kinetic) arheotrope: (○) unstable node, (□) saddle point, (●) stable node.

These singular point branches approach the (reactive) azeotropes if the pore diameter is larger than a few microns. In this situation, the membrane does not induce any additional selectivity to the separation process. If the pore diameter is less than a few nanometers, the membrane induces the maximum additional selectivity which is exerted by Knudsen diffusion as accounted for in the dusty gas model.

4. Conclusions

In this work, a model is formulated for the feasibility analysis of continuously operated membrane reactors. Two quaternary reaction systems are investigated as illustrative examples. In the first hypothetical system, it has been shown that a slightly selective membrane can change the locations of feasible product mixtures; the attainable mixtures are termed as *arheotropes*, meaning in translation "*the liquid composition is not changing with flux*". At higher selectivity, the membrane can even change the stability of arheotropes. This implies that desired product mixtures which are not attainable by distillation can be made attainable by application of suitable membranes.

Geometrically, the arheotropy condition for a quaternary system yields two surfaces in the composition space, and the intersection of these two surfaces determines the curve on which all potential singular points are located. Singular point analysis can be carried out not only with respect to the Damköhler number but also with respect to the property of the membrane. This gives valuable information on the selection of a suitable membrane. In the considered practical example, the esterification of acetic acid with propanol, the dusty gas model is applied to describe the diffusion through a porous polycarbonate membrane. The dusty gas model can be cast into an explicit form in which the apparent mass transfer matrix is non-diagonal and dependent on the state variables. Therefore, the proposed methodology is applicable not only to membranes with constant mass transfer matrices but also to real materials.

The presented analysis predicts the existence of reactive arheotropes in case of the acetic acid/propanol esterification. The experimental validation of this prediction is subject of our current research activities.

Acknowledgements

The authors would like to thank Mr. Valentin Chernev's support to this work during his stay in Magdeburg.

References

[1] Y. Zhu, H. Chen, J. Membr. Sci. 138 (1998) 123.
[2] J.M. van de Graaf, M. Zwiep, F. Kapteijn, J.A. Moulijn, Appl. Catal. A 178 (1999) 225.
[3] L. Domingues, F. Recasens, M.A. Larrayoz, Chem. Eng. Sci. 54 (1999) 1461.
[4] A.E.W. Beers, R.A. Spruijt, T.A. Nijhuis, F. Kapteijn, J.A. Moulijn, Catal. Today 66 (2001) 175.
[5] E. Piera, C. Tellez, J. Coronas, M. Menendez, J. Santamaria, Catal. Today 67 (2001) 127.
[6] K. Tanaka, R. Yoshikawa, C. Ying, H. Kita, K.-I. Okamoto, Catal. Today 67 (2001) 121.
[7] M.P. Bernal, J. Coronas, M. Menendez, J. Santamaria, Chem. Eng. Sci. 57 (2002) 1557.
[8] J.J. Jafar, P.M. Budd, R. Hughes, J. Membr. Sci. 199 (2002) 117.
[9] X. Feng, R.Y.M. Huang, Chem. Eng. Sci. 51 (1996) 4673.
[10] W.S. Moon, S.B. Park, J. Membr. Sci. 170 (2000) 43.
[11] S.Y. Lim, B. Park, F. Hung, M. Sahimi, T.T. Tsotsis, Chem. Eng. Sci. 57 (2002) 4933.
[12] S. Assabumrungrat, W. Kiatkittipong, P. Praserthdam, S. Goto, Catal. Today 79–80 (2003) 249.
[13] Y.-S. Huang, K. Sundmacher, Z. Qi, E.-U. Schlünder, Chem. Eng. Sci. 59 (2004) 2863.
[14] Y.-S. Huang, K. Sundmacher, S. Tulashie, E.-U. Schlünder, Chem. Eng. Sci. 60 (2005) 3363.
[15] Z. Qi, D. Flockerzi, K. Sundmacher, AIChE J. 50 (2004) 2866.
[16] E.A. Mason, A.P. Malinauskas, Gas transport in porous media: the dusty gas-model, Elsevier, Amsterdam, 1983.
[17] R. Krishna, J.A. Wesselingh, Chem. Eng. Sci. 52 (1997) 861.
[18] R.C. Reid, J.M. Prausnitz, B.E. Poling, The Properties of Gases and Liquids, McGraw-Hill, New York, 1987.
[19] D. Barbosa, M.F. Doherty, Chem. Eng. Sci. 43 (1988) 529.
[20] D. Barbosa, M.F. Doherty, Chem. Eng. Sci. 43 (1988) 541.
[21] J. Marek, G. Standart, Colln. Czech. Chem. Commun., Engl. Edn. 19 (1954) 1074.
[22] J. Gmehling, U. Onken, Vapour–liquid equilibrium data collection, chemistry data series, Frankfurt am Main, DECHEMA, 1977.